Phase diagram, structure, and magnetic properties of the Ge-Mn system: A first-principles study

Emmanuel Arras, Damien Caliste, Thierry Deutsch, Frédéric Lançon, and Pascal Pochet*
Laboratoire de Simulation Atomistique (L_Sim), SP2M, INAC, CEA-UJF, F-38054 Grenoble Cedex 9, France
(Received 17 September 2010; revised manuscript received 23 December 2010; published 6 May 2011)

We study the whole Ge-Mn phase diagram with density functional theory (DFT) methods. The 16 known phases are described and trends are analyzed. The compounds are then simulated, allowing a complete evaluation of this method in the projector augmented-wave approach within the collinear spin-polarized framework. Structural parameters, as well as magnetic properties, are compared to experimental values. Stability issues are addressed using a thermodynamic approach based on the grand potential, showing good agreement with experimental data. The impact of semicore electrons and the exchange-correlation functional are also discussed. Finally, it is shown that DFT methods are well suited to study this system, provided that the generalized gradient approximation is used, as opposed to the local density approximation, and correlations between structural errors and Mn concentration are taken into account. In addition, the precision achieved when compared to experiments is 40 meV/atom on energy, ±3% on the lattice parameter, and $0.2\mu_B$/Mn on magnetic moments. Magnetic orders are mostly well reproduced.

DOI: 10.1103/PhysRevB.83.174103 PACS number(s): 71.15.Dx, 75.50.Pp, 31.15.A−

I. INTRODUCTION

Spintronics appeared from the start as a very promising way to improve electronic devices. However, if significant breakthroughs were made, its full potential is still to be achieved. The bottleneck is the lack of suitable materials allowing simultaneous control over electric and magnetic properties. Encouraging experimental results reported by Park *et al.*[1] have drawn attention to the promising Ge-Mn system, leading to a large variety of new experimental results.[2–7] On the other hand, density functional theory (DFT) calculations were extensively used in theoretical works[8–15] to support, explain, and explore this complex system. Yet no complete study was performed to assess the relevance of DFT calculations in this case, and only limited comparisons have been proposed.[10,11,13] Moreover, one of the key results of these methods, the total energy, is at the same time the least efficiently used. This is all the more puzzling because it is of particular importance in this research where out of equilibrium techniques are widely used to obtain new interesting metastable compounds. We propose in this paper a general approach to evaluate the prediction capabilities of a simulation method, as well as a thermodynamic model to address the stability issues between phases. The successful application of our approach to the complex Ge-Mn system is an indication of its relevance for other spintronic-relevant systems. The paper is organized as follows: Methodological details are given first, then the known phases are reported and described, and finally experimental and numerical results are compared regarding structural, magnetic, and stability properties.

II. METHODOLOGICAL DETAILS

A. Method generalities

We have used the projector augmented-wave (PAW) approach as implemented in the ABINIT code,[16,17] within the generalized gradient approximation[18] (GGA), for the exchange-correlation energy in the collinear spin-polarized DFT framework. Two sets of pseudopotentials were generated both for Mn and Ge, using the ATOMPAW code.[19] Without semicore electrons, the first set includes only 4*s* and 4*p* states as valence electrons for Ge and 4*s* and 3*d* states for Mn, with augmentation radii of, respectively, 1.22 and 1.16 Å. Semicore electrons are added in the second set (3*d* for Ge; 3*s* and 3*p* for Mn) with an augmentation radius of 1.16 Å for both. Completeness of the basis set were ensured for each pseudopotential. Local density approximation (LDA) pseudopotentials were also generated with the same parameters for comparison. The impact of semicore electrons has been evaluated by comparing the results when either all semicore electrons (for both Mn and Ge) or none are frozen. We note that the computation time is almost ten times larger in the second case as compared to the first one, mainly because of three reasons: (i) A cutoff energy of 20 Ry is sufficient without semicore electrons, while 35 Ry is required with them; (ii) the higher number of electron bands; and (iii) the number of iterations to achieve convergence is larger because of the increase in degrees of freedom.

During the process of testing our pseudopotentials, and comparing them to the literature, we have observed that both Hartwigsen-Goedeker-Hutter (HGH)[20] and HGH-Krack[21] pseudopotentials of manganese with frozen semicore electrons (Q7) are inappropriate with a wrong degeneracy of the empty 3*d* levels (see Fig. 1), but more importantly the cohesive energy of the Mn γ phase is found to be negative (−1.23 eV/Mn, i.e., unstable), when it should be positive, as observed with all other pseudopotentials [for instance, +4.67 eV/Mn for HGH with unfrozen semicore electrons (Q15) in LDA, denoted as HGH Q15 in Fig. 1].

B. Simulation parameters used for all Ge-Mn compounds

For the simulations of all the Ge-Mn compounds, we have used *k*-point meshes that ensure an error on the total energy lower than 0.1 meV/atom. Also, a Fermi-Dirac smearing with a temperature of 300 K was applied to improve convergence.[22] Internal coordinates as well as lattice parameters were relaxed simultaneously until achieving convergence of better than 10^{-4} Hartree Bohr^{-1} on forces and 10^{-3} GPa on pressures.

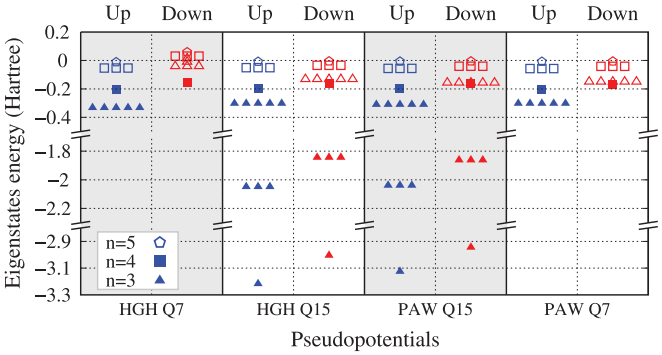

FIG. 1. (Color online) Energy levels of one Mn atom in vacuum, depending on the pseudopotential (LDA). Filled and hollow symbols correspond to filled and empty states, respectively. Triangles correspond to the state with a principal quantum number $n = 3$, squares to $n = 4$, and pentagons to $n = 5$. Results of HGH pseudopotentials and our PAW pseudopotentials are detailed both with (Q15) and without (Q7) semicore electrons taken in valence. Spin-*up* states are in blue whereas spin-*down* states are in red. One can observe that the HGH-Krack pseudopotential without semicore electrons (HGH Q7) leads to excited $3d$ levels that do not have the correct degeneracy.

Our tests show this corresponds to a precision of better than 0.1 meV/atom on energy and 0.01% on the lattice parameter.

Different magnetic orders were tested for each compound.[23] For phases exhibiting noncollinear magnetism, different projections of magnetic moments were used as the starting point for the calculations. In this case, the results presented here correspond to the lowest-energy configuration.

III. THE KNOWN Ge-Mn COMPOUNDS

A. Different phases in different thermodynamic conditions

We have studied all the Ge-Mn phases present in the (T,[Mn]) phase diagram of the GeMn binary alloy.[24] This diagram presents 12 defined compounds. Among them, six are stable under the standard conditions of temperature and pressure (STP): diamond Ge, $Mn_{11}Ge_8$ (θ), Mn_5Ge_3 (η), Mn_5Ge_2 (κ), Mn_3Ge (ϵ_1) and Mn_α and six others appear at high temperature: Mn_2Ge (χ), Mn_5Ge_2 (ζ), Mn_3Ge (ϵ), Mn_β, Mn_γ, and Mn_δ.

However, this phase diagram only reports the variations of stoichiometry and temperature, whereas pressure is not taken into account. Yet, for the past 20 years, high-pressure synthesis of new compounds have been performed. Indeed, Takizawa *et al*. have managed to stabilize four new phases using a liquid melt of Ge and Mn at a pressure ∼4–6 GPa. These compounds are $MnGe_4$, Mn_3Ge_5, MnGe, and Mn_3Ge.

The 16 compounds just mentioned are further detailed in Table I, and shown in Fig. 2. We will now briefly described all these compounds and their particularities, starting with those stable in standard conditions, then high-temperature compounds, and finally high-pressure compounds.

B. Phases description

1. *Standard conditions for temperature and pressure (STP)*

(a) Diamond Ge. The stable phase of germanium is the diamond structure, which can be seen as the assembly of two face-centered cubic sublattices. Its properties have been thoroughly studied, experimentally as well as theoretically. Thus we will not describe it further.

TABLE I. The different phases of the GeMn binary alloy, and their characteristics. Magnetic orders can be ferromagnetic (FM), antiferromagnetic (AF), ferrimagnetic (FiM), noncollinear magnetic (NC), and nonmagnetic (NM). Most of the data are drawn from Refs. 25 and 26.

Compound	[Mn]		Pearson's symbol	Space group	Struct. design.	Prototype	Magnetic order	N_{atom}/ unit cell
STP	Diamond Ge	0%	cF8	$Fd\bar{3}m$	$A4$	C(diam)	NM	2
	$Mn_{11}Ge_8$ (θ)	57.9%	oP76	$Pnma$		$Mn_{11}Cr_8$	NC	76
	Mn_5Ge_3 (η)	62.5%	hP16	$P6_3/mcm$	$D8_8$	Mn_5Si_3	FM	16
	Mn_5Ge_2 (κ)	71.4%	oI28	$Ibam$		Mn_5Ge_2	FiM	28
	Mn_3Ge (ϵ_1)	75%	tI8	$I4/mmm$	$D0_{22}$	Al_3Ti	FiM	4
	Mn_α	100%	cI58	$I\bar{4}3m$	$A12$	αMn	NC	58
HT	Mn_2Ge (χ)	66.7%	hP6	$P6_3/mmc$	$D8_2$	Ni_2In	FiM	6
	Mn_5Ge_2 (ζ)	71.4%	hp128	$P3c1$			AF	42
	Mn_3Ge (ϵ)	75%	hP8	$P6_3/mmc$	$D0_{19}$	Ni_3Sn	NC	8
	Mn_β	100%	cP20	$P4_132$	$A13$	βMn	NC	20
	Mn_γ	100%	cF4	$Fm\bar{3}m$	$A1$	Cu	–	1
	Mn_δ	100%	cI2	$Im\bar{3}m$	$A2$	W	–	2
	$Mn_{\gamma-\delta}$[a]	100%	tI2	$I4/mmm$	$A6$	In		2
HP	$MnGe_4$	18.0%	cI10	$I432$		Hg_4Pt[b]	FM	39
	Mn_3Ge_5	37.5%	oP[c]	D^8_{2d}				32[c]
	MnGe	50%	cP8	$P2_13$	$B20$	FeSi	AF	8
	Mn_3Ge	75%	cP4	$Pm\bar{3}m$	$L1_2$	Cu_3Au	FM	4

[a]$Mn_{\gamma-\delta}$ is the low-temperature form of both Mn_γ and Mn_δ phases (Ref. 27).
[b]The $MnGe_4$ compound is built from four faulted Hg_4Pt unit cells.
[c]Deduced from our simulations, since atomic coordinates are not known experimentally.

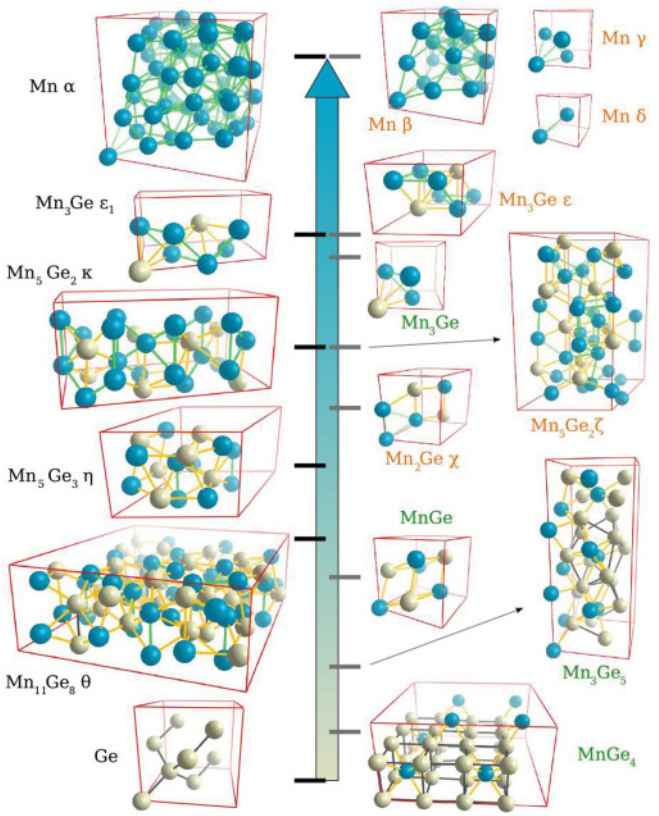

FIG. 2. (Color online) The known Ge-Mn compounds, ranging from 0% Mn at the bottom to 100% Mn at the top. Crystal lattices are shown, with, on the left-hand side, stable phases in the standard conditions of temperature and pressure (STP), and on the right-hand side, high-temperature (HT) compounds in orange and high-pressure (HP) compounds in green.

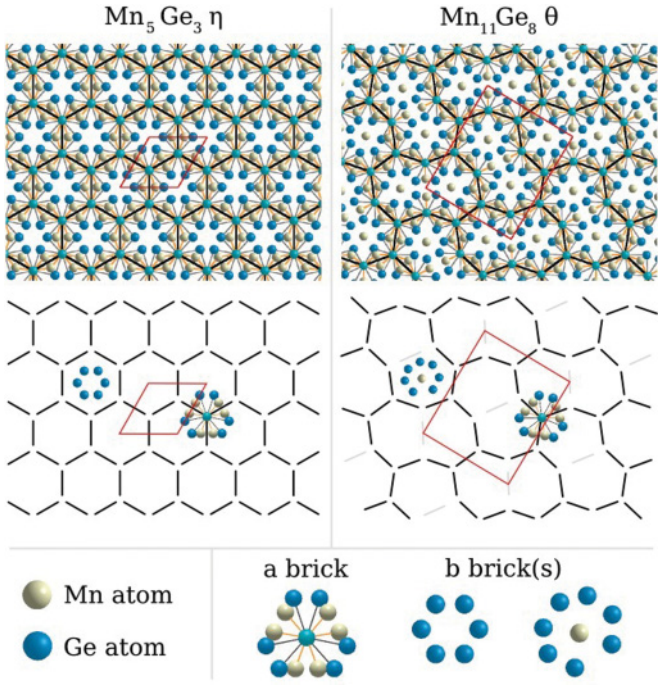

FIG. 3. (Color online) Comparison between Mn_5Ge_3 (η) and $Mn_{11}Ge_8$ (θ) structures, from the c axis. Shown in red are the unit cells. The a brick is the same in the two compounds, whereas the b bricks are different. The hexagonal and "bean-shaped" organization of bricks a are also shown in Mn_5Ge_3 (η) and $Mn_{11}Ge_8$ (θ) compounds, respectively.

(b) $Mn_{11}Ge_8$ (θ). The $Mn_{11}Ge_8$ compound (sometimes referred to as Mn_3Ge_2 for historical reasons) is the stable GeMn alloy containing the fewest Mn atoms, although still 58%. Due to this feature, the compound segregates and forms clusters when annealing GeMn diluted magnetic semiconductor (DMS), which have lower global concentrations.

It was identified in 1974 to be isostructural to $Mn_{11}Cr_8$.[28] Its unit cell contains 76 atoms, and despite an apparent strong complexity, it can be understood by comparing it to Mn_5Ge_3. Indeed, both compounds are built from the same brick (brick a on Fig. 3). The difference comes from the brick b (see Fig. 3) which is made of six Mn atoms in Mn_5Ge_3, when there are seven Mn atoms and two Ge atoms in $Mn_{11}Ge_8$. Thus, a bricks are organized on an hexagonal lattice for the Mn_5Ge_3, and as "beans" in $Mn_{11}Ge_8$ (see Fig. 3). In the same way that Mn atoms are described in Mn_5Ge_3, Mn_I are at the center of a bricks, and Mn_{II} form the b bricks.

The magnetism of this compound is also peculiar. It is antiferromagnetic (AF) at low temperature, becomes ferromagnetic above 150 K, and then paramagnetic beyond 274 K.[29] However, the atomic magnetic moments are only known to be in the **a**–**c** plane in the collinear AF order, while the ferromagnetic order appears with an atomic magnetic moment of $0.05\mu_B$/Mn in the **b** direction.[29] Yet, the paramagnetic moment reaches $3.26\mu_B$/Mn. Thus it is believed that the ferromagnetism is due to a small out-of-the-plane (**a**–**c** plane) contribution of atomic moments, in a configuration close to that of the AF order.[29] However, no further information is available.

(c) Mnd_5Ge_3 (η). The structure of this compound is identical to that of Mn_5Si_3,[30] yet it is ferromagnetic with a Curie temperature (T_C) of 300 K. It is of hexagonal symmetry, with a local order very close to that of $Mn_{11}Ge_8$, with a slightly higher Mn content. The unit cell is made of 16 atoms of three types: Mn_I and Mn_{II}, which exhibit a magnetic moment of $1.9\mu_B$ and $3.3\mu_B$, respectively,[31] and one type of Ge atoms.

(d) Mn_5Ge_2 (κ). The exact atomic structure of this compound has been determined in 1984,[32] but it was still referred to as Mn_7Ge_3 in 1990.[26] It is described as an arrangement of $4 \times 2 \times 2$ body-centered cubic cells (bcc), in which four atoms are removed (see Ref. 32). The unit cell thus contains 28 atoms: three types of Mn and one of Ge. It is ferrimagnetic with compensation temperatures of 395 and 710 K, respectively.[33,34] Mn atoms hold local moments of $2.18\mu_B$, $2.02\mu_B$, and $-2.96\mu_B$.[33,34]

(e) Mn_3Ge (ϵ_1). This phase is isostructural to Al_3Ti,[35] of face-centered tetragonal (fct) type. Its stoichiometry is closer to $Mn_{3.25}Ge$,[36] which is explained by the partial occupancy of the $2a$ site (6% Mn and 94% Ge).[33] It can also become $Mn_{3.4}Ge$ depending on preparation conditions.[26] In our calculations however, we have used a $2a$ site occupancy of 100% Ge (Mn_3Ge) for obvious simplicity reasons. This compound is ferrimagnetic,[33] with a sublattice of Mn holding a local

moment of $1.9\mu_B$ and the other of $-3\mu_B$, and a Curie temperature that is higher than the melting one.

(f) Mn α. The stable phase of pure manganese is extremely complex, as opposed to that of other transition metals that are all compact (fcc, hcp, or bcc). Fifty-eight atoms, divided into six sublattices, make the unit cell.[37] This complexity seems to have its origins in the competition between Hund's rule (that tends to maximize total spin moment) and orbital hybridization, with on top of that an AF triangular frustration.[11]

2. High-temperature phases

There are three known Ge-Mn compounds and three allotropic forms of Mn.

(a) Mn_2Ge (χ). This compound has no equivalent at low temperature, and breaks down to Mn_5Ge_3 (η) and Mn_5Ge_2 (κ) after annealing. The structure prototype is Ni_2In.[38] The cell consists of six atoms with two types of Mn. To our knowledge, local magnetic moments have not been measured yet.

(b) Mn_5Ge_2 (ζ). This is the high-temperature continuity of Mn_5Ge_2 (κ). It is in fact made of two phases: $Mn_{5.11}Ge_2$ ζ_1 (Ref. 39) and Mn_5Ge_2 ζ_2.[40] Both can be seen as faulted Mn_2Ge (χ),[36,41] but their unit cells contain 130 and 40 atoms, respectively. We have only simulated the smaller phase (ζ_2). Magnetism seems to be AF,[36] with no further details.

(c) Mn_3Ge (ϵ) This is the high-temperature phase of the Mn_3Ge (ϵ_1) compound. It is also referred to as $Mn_{3.4}Ge$,[26] which means some of the Ge atom sites are partially occupied by Mn, as for the ϵ_1 phase. The unit cell is made of six atoms. The magnetism is noncollinear, with an AF triangular interaction.[33] A weak ferromagnetism ($T_C = 365$ K) is observed along the easy magnetization axis out of the *ab* plane.[33]

(d) Mn β. The β phase of manganese ($T > 720\,^\circ$C) is close to the α phase, yet more ordered: The unit cell contains "only" 20 atoms of two sublattices.[42] The magnetism is also noncollinear AF.[10]

(e) Mn γ. The compact phase of manganese appears above 1100 °C.[26] It is a face-centered cubic structure (fcc), with one Mn atom per unit cell. It is paramagnetic at these high temperatures, with a magnetic moment of $2.3\mu_B$/Mn.[43,44]

(f) Mn δ. Beyond 1140 °C (and under the melting point) is the Mn_δ phase, of body-centered cubic structure (bcc).[26] Its magnetism is unknown.

(g) Mn γ − δ. This particular phase which does not appear on the phase diagram is the low-temperature form of γ and Mn δ when quenched. This face-centered tetrahedron (fct)[27] phase will be referred to as Mn $\gamma - \delta$. Very little information is available, and none regarding magnetism.

3. High-pressure phases

(a) $MnGe_4$. This phase forms under pressure higher that 5.5 GPa and temperatures ∼600–700 °C. The unit cell reported is made of four Hg_4Pt unit cells[45] with no further precision. The stoichiometry is closer to $Mn_{0.875}Ge_4$, which corresponds to one missing Mn in the 40-atom unit cell, as proposed in the original experimental study, thus making it Mn_7Ge_{32}. Since all Mn atoms are equivalent, we have, in our simulations, removed one Mn in the 40-atom unit cell. This compound is also known to be metastable in the STP conditions, and breaks down into Mn_5Ge_3 and diamond Ge at 300 °C. It is ferromagnetic with a T_C of 340 K and a magnetic moment of $1.2\mu_B$/Mn.

(b) Mn_3Ge_5. This phase appears at 4 GPa and between 600 and 1000 °C. Its local structure is close to that of Mn_4Si_7 or $Mn_{11}Si_{19}$, and more generally of the MGe_2 compounds with M = V, Cr, Mo, Ru, Rh.[46] However, atomic coordinates are not available, and we have been forced to guess them from known MGe_2 compounds. Fully relaxed results have proven to be quite satisfactory (stoichiometry, lattice parameters, and energy), as it will be shown later. The magnetic properties of this compound have not been experimentally studied.

(c) MnGe. The stoichiometric MnGe phase forms in similar conditions: 4–5.5 GPa, 600–1000 °C. It has the same B20 cubic unit cell[47] as many other semiconductor-transition metal alloys (FeGe, CrGe, and the prototype FeSi). Experimental measurements show an AF behavior, without further details.

(d) Mn_3Ge. This phase was identified in 2002.[48] It is stable under 6.2 GPa and 1000 °C. The type is fcc $L1_2$ (prototype Cu_3Au). Its local structure is close to that of Mn_3Ge ϵ_1. It is ferromagnetic, the saturated magnetic moment reaches $0.87\mu_B$/Mn, and the Curie temperature is 400 K.

C. Evolution of the compacity of Ge-Mn phases

Let us first discuss some trends about all these compounds. Germanium and manganese have very different features: The first one is a semiconductor which binds covalently with (optimally) four neighbors, whereas the second one is a metal that maximizes its number of neighbors. In one case, the stable structure is open (diamond Ge), while in the second case it is compact [Mn α (Ref. 11)]. There is thus an impact on the evolution of the atomic density of GeMn alloys versus the Mn concentration. As plotted in Fig. 4, we can see that it almost doubles from pure Ge to pure Mn, with a strong increase at low Mn concentration. In addition, it must be noted that this tendency is not due to the atomic radius of atoms, since Mn atoms are bigger (1.4 Å) than Ge atoms (1.23 Å), but due to the crystallographic ordering.

This density variation is significant information for the research of new metastable compounds[50] formed at the low-temperature growth of Ge-Mn samples. This must also be taken

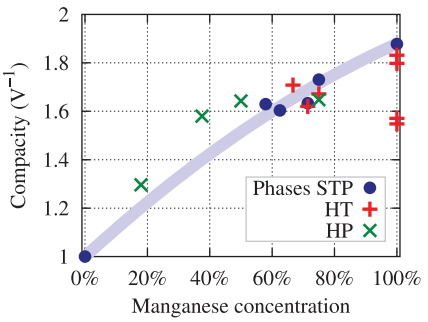

FIG. 4. (Color online) Evolution of the experimental compacity (Ref. 49) of GeMn alloys as a function of Mn concentration. Results are normalized to one for diamond Ge. Disks are STP phases, whereas crosses are HT or HP phases, red and green, respectively. The line is a guide for the eyes and emphasizes the strong correlation between compacity and Mn concentration.

into account when evaluating the Mn concentration of GeMn clusters of unknown crystal structure.[4–6]

The two pure Mn phases with a compacity lower than 1.6 are Mn γ and δ. This difference with Mn α, β and γ-δ comes from thermal expansion, since measurements were performed at high temperature, respectively, 1100 and 1140 °C.

IV. *Ab initio* STUDY OF THE Ge-Mn COMPOUNDS

After a review of the known Ge_xMn_{1-x} alloys of the (x,T,P) phase diagram, we will apply first-principles methods (described in Sec. II) to compare experimental and numerical results regarding structural, magnetic, and stability properties. Moreover, the impact of the semicore electrons will be evaluated.

A. Structure: Lattice parameters and internal relaxation

Simulated and experimental lattice parameters of all phases are reported in Table II. Our results are consistent with the published studies using the same approximations (DFT-GGA): Differences are lower than 0.2% for diamond Ge,[51] Mn_5Ge_3,[52] and Mn α,[11] and 0.6% for Mn β.[10] Shown in Table II and plotted in Fig. 5 versus the Mn concentration, the mean error Err_{tot} on the lattice parameters is computed from the unit-cell volume V as follows:

$$Err_{tot} = \left(\frac{V_{cal}}{V_{exp}}\right)^{\frac{1}{3}} - 1. \quad (1)$$

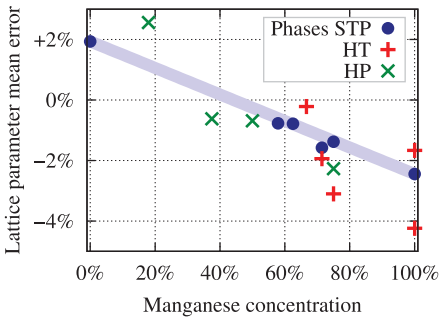

FIG. 5. (Color online) Evolution of the error Err_{tot} on the lattice parameters calculated by the DFT method, vs Mn concentration, for simulations without the semicore electrons. Disks are STP phases, whereas crosses are HT or HP phases, red and green, respectively. A straight line is drawn between diamond Ge and Mn α to emphasizes the trend.

The first thing that can be noticed from Fig. 5 is the strong correlation between the Mn concentration and the lattice parameter error, which seems to be quasilinear for the STP compounds. It is tempting to explain this phenomenon simply by stating that the Ge atom size is overestimated by 2%, and the Mn atom size underestimated by 3%. However, details of both internal and cell relaxations prove otherwise, and point toward a more complex phenomenon.

In the case of metastable compounds (HT and HP phases), the linear correlation seems to apply to a lesser extent. This can however be explained as follows: (i) Simulation does not respect the precise stoichiometry of some compounds [e.g.,

TABLE II. Comparison of simulated and experimental lattice parameters of known Ge-Mn compounds. Simulation data were obtained in the magnetic ground state.

		Experimental lattice parameter (Å)				Simulation (this study) lattice parameter (Å)				
	Compound	a	b	c	Ref.	a (err)[a]	b (err)[a]	c (err)[a]	Err_{tot}[a]	Err_{tot}[b]
STP	Diamond Ge	5.66			53	5.77 (+1.9%)			+1.9%	+1.9%
	$Mn_{11}Ge_8$ (θ)	13.17	15.82	5.07	54	13.11(−0.5%)	15.61(−1.3%)	5.04(−0.5%)	−0.8%	−0.3%
	Mn_5Ge_3 (η)	7.18		5.05	25	7.15(−0.5%)		4.99(−1.3%)	−0.8%	−0.3%
	Mn_5Ge_2 (κ)	11.78	5.37	6.14	25	11.55(−2.0%)	5.30(−1.3%)	6.05(−1.5%)	−1.6%	−1.2%
	Mn_3Ge (ϵ_1)	2.69		3.62	25	2.65(−1.4%)		3.57(−1.4%)	−1.4%	−1.1%
	Mn_α	8.88			37	8.66(−2.4%)			−2.4%	
HT	Mn_2Ge (χ)	4.17		5.28	25	4.25(1.8%)		5.06(−4.1%)	−0.2%	0.4%
	Mn_5Ge_2 (ζ)	7.20		13.08	55	7.08(−1.7%)		12.76(−2.4%)	−1.9%	
	$Mn_{3.4}Ge$ (ϵ)	5.35		4.37	55	5.17(−3.2%)		4.25(−2.9%)	−3.1%	−3.0%
	Mn_β	6.31			27	6.05(−4.2%)			−4.2%	−4.2%
	Mn_γ	3.86[c]			27	3.54(−8.4%)			−8.4%	−8.4%
	Mn_δ	3.08[d]			27	2.80(−9.3%)			−9.3%	−9.1%
	$Mn_{\gamma-\delta}$	2.67		3.46	27	2.60(−2.8%)		3.48(+0.7%)	−1.7%	−1.7%
HP	$MnGe_4$	11.03	11.03	5.60	45	11.35(2.9%)	11.35(2.9%)	5.71(1.9%)	2.6%	2.9%[e]
	Mn_3Ge_5	5.75		13.89	46	5.71(−0.7%)		13.82(−0.5%)	−0.6%	
	MnGe $B20$	4.80			47	4.76(−0.7%)			−0.7%	−0.2%
	Mn_3Ge $L1_2$	3.80			48	3.75(−1.5%)	3.75(−1.5%)	3.65(−3.9%)	−2.3%	−1.9%

[a]Without semicore electrons.
[b]With semicore electrons.
[c]Measured at 1100 °C.
[d]Measured at 1140 °C.
[e]Extrapolated from the $NiHg_4$ for the calculation with semicore electrons.

$Mn_{3.4}Ge$ (ϵ), $Mn_{5.11}Ge_2$ (ζ), . . .]; (ii) there are compounds not fully characterized experimentally, from a magnetic or structural point of view ($MnGe_4$, Mn_3Ge_5, Mn_3Ge ϵ), leading to possible errors in our simulations; (iii) noncollinear magnetism is not well simulated; (iv) temperature effects are not included in the calculations; and finally (v) experimental data are also subject to errors, especially in nonstandard conditions.

Nevertheless, the $MnGe_4$ compound is noticeably far of the straight line underlying the tendency in Fig. 5. The error on the lattice parameter is indeed of 2.6% (2.9% with semicore electrons). We think it can only be attributed to the atomic structure, which must be erroneous. However, the hypothesis we have done on the structure (removal of one Mn interstitial atom) is the only one possible, and is in full agreement with the experimental description of Ref. 45.

It is also worth noticing that the high-pressure Mn_3Ge $L1_2$ cubic symmetry is broken in the calculated structure. This is due to the fact that we could not reproduce the noncollinearity of the experimental magnetic order. Instead, a simple AF order corresponds to the lowest energy, but breaks the symmetry.

With the tendency shown in Fig. 5, it seems possible to estimate the error Err_{tot} coming from the method for other concentrations than those already simulated. In the range 30%– 50%, for example, the error seems minimal because of the compensating errors of Mn and Ge. Thus in this range one would have to compare the simulated lattice parameters directly with the experimental values, instead of applying a correction deduced from a simulation of Ge diamond.

The origin of this surprising behavior of Mn in GGA (that usually overestimates lattice parameters) can be attributed to the exchange and correlation mechanisms. Indeed, they are of particular importance for Mn where the d shell is half filled, i.e., the worst case for local or quasilocal approximations. We also think that GGA must therefore be preferred to LDA when it comes to simulating these compounds, especially when magnetic properties are involved, since magnetism is known to be strongly dependent on interatomic distances.

B. Magnetism

The next discussion is about magnetic properties, and especially magnetic order and local moments. Experimental and numerical values are reported in Table III. Theoretical values are calculated as the difference between *up* and *down* electron density inside spheres centered on nuclei, and of radius 1.17 Å (PAW spheres). As mentioned before, these data are obtained for simulations where both internal coordinates and cell parameters are fully relaxed. Again, these values are consistent with those already published,[10,11,52] with an agreement of better than $0.2\mu_B$/Mn.

First, the magnetic configurations with the lowest energies are indeed those measured experimentally, except for two high-pressure configurations and of course for the four noncollinear configurations since they could not be considered here. These six latter configurations, as well as the experimentally unknown configurations, will be discussed afterward. The second agreement concerns the amplitude of the magnetic moments, which are relatively well reproduced: The mean error is lower than $0.3\mu_B$/Mn for STP phases. Regarding HT and HP phases, it appears that the larger errors are due to the strong impact of the lattice parameter errors on the magnetic properties. Indeed, calculations done by imposing the experimental values for the lattice parameters lead to much better agreements.[10] For Mn_γ and Mn_δ, the experimental magnetic moment values were

TABLE III. Comparison between experimental and simulated values of local magnetic orders and local magnetic moments, in Bohr magneton (μ_B). Magnetic orders can be ferromagnetic (FM), antiferromagnetic (AF), ferrimagnetic (FiM), and noncollinear magnetic (NC).

		Experiment					Simulation (this study)						Mean
	Compounds	Magn. order	Mn_1	Mn_2	Mn_3	Ge/Mn_4	Ref.	Magn. order	Mn_1	Mn_2	Mn_3	Ge/Mn_4	error[a]
STP	$Mn_{11}Ge_8$ (θ)	NC					29	AF or FM[b]	2.3	2.7		−0.14	
	Mn_5Ge_3 (η)	FM	1.9	3.3			31	FM	2.2	3.1		−0.15	0.27
	Mn_5Ge_2 (κ)	FiM	2.0	2.2	−3.0		34	FiM	1.7	2.0	−3.1	−0.02	0.19
	Mn_3Ge (ϵ_1)	FiM	3.0	−1.9			33	FiM	2.9	−2.0		0.05	0.09
	Mn_α	NC	2.8	−1.8	0.5	0.48	37	FiM	3.0	−2.3	0.5	−0.15	0.24
HT	Mn_2Ge (χ)							FiM	2.9	−2.0		0.01	
	Mn_5Ge_2 (ζ)	AF					36	AF-FiM[c]	∼2.5				
	$Mn_{3.4}Ge$ (ϵ)	NC	2.4				33	FiM	2.0				0.42
	Mn_β	NC	−0.2	1.0			61	FiM	−0.2	0.5			0.29
	Mn_γ		2.3[d]				43	AF	0.9				1.4
	Mn_δ		∼1[d]				43	NM	0				1
	$Mn_{\gamma-\delta}$							AF	1.9				
HP	$MnGe_4$	FM	1.2				45	FM	2.5				1.33
	Mn_3Ge_5							AF	∼1.1				
	MnGe $B20$	AF	3.0				47	FM	2.2				0.8
	Mn_3Ge $L1_2$	FM	0.9				48	FiM	2.9	−2.2	−2.2		0.34

[a] $Err_{moy} = \langle||\mu_i^{simu}| - |\mu_i^{expe}||\rangle$.

[b] AF or FM: The ferromagnetic and several antiferromagnetic orders are close by less than 10 meV/atom.

[c] AF-FiM: Local order is ferrimagneticlike Mn_2Ge (χ), but different variants lead to a total moment close to 0.

[d] μ_C: Magnetic moment in the paramagnetic regime, measured for the high-temperature lattice parameter.

obtained in the paramagnetic regime,[56,57] i.e., with a much higher lattice parameter due to thermal expansion. The case of $MnGe_4$ is finally again problematic since the error on magnetic moment reaches $1.3\mu_B$/Mn. We will now discuss each of the nine phases whose magnetic order is either noncollinear or unknown, as well as the two configurations for which the simulation does not reproduce the experimental results.

(a) $Mn_{11}Ge_8$ (θ). Its magnetic order being noncollinear,[29] we have tested four different configurations: (i) ferromagnetic; (ii) ferrimagnetic, with Mn_I *up* and Mn_{II} *down*; and (iii) two AF configurations, in which parallel alignment is preserved inside *b* bricks,[58,59] and these bricks are antiferromagnetically coupled to each other. As a result, ferromagnetic atoms are gathered in slices, as suggested experimentally.[60] The least stable configuration is the ferrimagnetic one, almost 20 meV/atom higher than the three others, which are degenerated within a few meV. The lowest energy corresponds to one of the AF configurations, which as been reported in Table III. Lattice parameters can change by almost 1% depending on the magnetic order.

(b) Mn_α and Mn_β. They display experimentally a frustrated AF behavior. We have used the collinear configurations proposed in Refs. 10 and 11, which correspond as closely as possible to their magnetic order.

(c) Mn_2Ge (χ). Its magnetic order is unknown experimentally. The lowest energy found corresponds to a ferrimagnetic order with a ferromagnetic alignment inside each sublattice.

(d) Mn_5Ge_2 (ζ). Its magnetic order is also unknown experimentally. It was simulated in a ferrimagnetic configuration close to that of Mn_2Ge (χ), since the two structures have a similar local order.[41] However, due to the different variants present in the ζ phase, the total magnetic moment is close to zero.

(e) $Mn_{3.4}Ge$ (ϵ). It has been reported as a noncollinear antiferromagnetic, with triangular spin arrangements. The lowest energy found corresponds to an AF order that preserves the cell symmetry: One Mn triangle is *up* whereas the other one is *down*.

(f) Mn_γ. The magnetic order of this high-temperature compound has not been unraveled experimentally, probably because of its instability at low temperature.[27] We find it to be antiferromagnetic of AuCu type, as reported by Hobbs *et al.*[10] Both ferromagnetic and [111]-oriented antiferromagnetic have higher energies.

(g) Mn_δ. For the same reason as Mn_γ, experimental data are not available. Mn_δ seems however to be ferromagnetic in simulation, with an extremely low magnetic moment, thus making it almost nonmagnetic.

(h) Mn_3Ge_5. Our calculations show that a ferrimagnetic configuration is the most stable one, as compared to ferromagnetic order, as well as antiferromagnetic by plane and by columns.

(i) Mn_3Ge $L1_2$. This compound is ferrimagnetic in simulation, whereas it is described as ferromagnetic experimentally.[48] However, experimental results mention a strong difference between the saturation magnetic moment μ_S ($0.9\mu_B$) and the paramagnetic moment μ_C ($1.7\mu_B$). Authors ascribe this difference to the itinerant ferromagnetism of the compound. Thus, either simulation fails to reproduce the correct magnetic order, or the experimental results are the consequence of a noncollinear magnetism, with an out-of-plane contribution as is the case for $Mn_{11}Ge_8$ or Mn_3Ge (ϵ).

(j) MnGe $B20$. The stoichiometric compound has the lowest energy in the ferromagnetic state, whereas experiment reveal an AF behavior. Yet, we have tested all possible magnetic configuration within the eight-atom unit cell, as well as for a supercell double the size. We see three possible explanations: (i) The magnetic configuration is more complex than we can handle, namely, it involves noncollinearity and/or periodicity bigger than two times the unit cell (e.g., spin spiral); (ii) method-induced relaxations change the sign of the interactions; and (iii) the exchange-correlation functional is particularly not adapted to this particular case.

(k) $MnGe_4$. The high-pressure Ge-rich compound again shows a large error in magnetic moments, which cannot solely be attributed to the error on the lattice parameter.

Lastly, the impact of semicore electrons on magnetism is minimal, since we find a mean difference between the two methods of lower than $0.1\mu_B$/Mn for all compounds.

C. Energy and stability

Energy is a key output of first-principles calculations, and a comparison of energies is used to assess the stability of a wide variety of chemical and structural configurations. Here, we want to compare the energies of the different Ge_cMn_{1-c} compounds, where c can vary from 0 to 1. The goal is to be able to predict which phases are stable, which are not, and most importantly, by what amount.

(a) *Theoretical basis.* A mere comparison of the total energy per atom is, however, impossible since two different species with different concentrations are involved in the compounds. We will use a semigrand canonical potential, similar to the one in Ref. 62, particularly convenient to study the equilibrium of systems that can exchange particles and thus the respective stability of each compound. Because our first-principles calculations have been done at $T = 0$ and with a crystal cell optimization that allows us to get energy at zero stress tensor $\boldsymbol{\tau}$ (in particular, at pressure $p = 0$), we will omit the temperature-entropy term TS and the $V\boldsymbol{\tau}\boldsymbol{\eta}$ term in the internal energy U,

$$U(\{N_i\}) = \sum_i \mu_i N_i, \tag{2}$$

where N_i is the number of atoms of type i and μ_i is their chemical potential. In our case, the sum is performed on the two different species of the system ($i \in \{\mathrm{Ge,Mn}\}$) and U is determined by the DFT calculations, $U = N\epsilon$, where ϵ is the computed energy per atom. To focus on the compound composition, it is convenient to make a simple change of variables and express the energy versus the total number of atoms $N = N_{\mathrm{Ge}} + N_{\mathrm{Mn}}$ and the difference $X = (N_{\mathrm{Ge}} - N_{\mathrm{Mn}})/2$:

$$U(\{N_i\}) = E(X,N) = -\Delta_\mu X + \overline{\mu} N, \tag{3}$$

where $\Delta_\mu = \mu_{\mathrm{Mn}} - \mu_{\mathrm{Ge}}$ is the chemical potential difference between Ge and Mn atoms, and $\overline{\mu}$ is the mean value $(\mu_{\mathrm{Ge}} + \mu_{\mathrm{Mn}})/2$. We now define the semigrand canonical potential

$\Phi(\Delta_\mu, N)$ using a Legendre transform[63,64] of E to get the intensive variable Δ_μ as state variable rather than X:

$$\Phi(\Delta_\mu, N) = E + \Delta_\mu X. \tag{4}$$

Although omitted in our notation, the transformation is also done for the conjugate variables (T,S) and $(\boldsymbol{\tau}, V\boldsymbol{\eta})$ in order to be able to impose the $T = 0$ and $\boldsymbol{\tau} = 0$ conditions. The only extensive state variable is now N and we can introduce some atomic quantities: the reduced semigrand canonical potential,

$$\phi(\Delta_\mu) = \Phi(\Delta_\mu, N)/N = \epsilon + \Delta_\mu x, \tag{5}$$

the *ab initio* energy per atom ϵ, and the deviation $x = X/N$ $(= c_{\mathrm{Ge}} - \frac{1}{2} = \frac{1}{2} - c_{\mathrm{Mn}})$, where c_{Ge} and c_{Mn} are the concentration of each specie (they abide by the relation $c_{\mathrm{Ge}} + c_{\mathrm{Mn}} = 1$). For a given value of the state variable Δ_μ, we want to determine which alloy has the lower potential $\phi(\Delta_\mu)$. From Eq. (5), we see that each compound γ defines a straight line $\epsilon_\gamma + \Delta_\mu\ x_\gamma$ in the $(\phi,\ \Delta_\mu)$ plane, where the energy ϵ_γ and the concentration deviation x_γ are characteristics of γ (see, for instance, Fig. 6). Therefore, in the graph ϕ vs Δ_μ, a stable alloy corresponds to its straight-line segment that is below all the other straight lines of the other compounds. Such a line segment represents a domain $[\Delta_\mu^{\min}, \Delta_\mu^{\max}]$ in which the phase is stable.

Because the Gibbs phase rule limits the number of independent intensive variables, $\overline{\mu}$ depends on Δ_μ, T, and $\boldsymbol{\tau}$. The last two intensive variables being set to zero in our case, the relation between $\overline{\mu}$ and Δ_μ can be found from the partial derivative equality[65]

$$\left.\frac{\partial E}{\partial N}\right|_X = \left.\frac{\partial \Phi}{\partial N}\right|_{\Delta_\mu}, \tag{6}$$

and from Eqs. (3) and (5),

$$\overline{\mu} = \phi. \tag{7}$$

Thus $\overline{\mu}$ is equal to $\epsilon + \Delta_\mu x$. The individual chemical potentials of any stable phase γ can be easily deduced:

$$\mu_{\mathrm{Ge}} = \epsilon_\gamma - c^\gamma_{\mathrm{Mn}}\Delta_\mu, \tag{8}$$

$$\mu_{\mathrm{Mn}} = \epsilon_\gamma + c^\gamma_{\mathrm{Ge}}\Delta_\mu. \tag{9}$$

For the pure Ge phase, $\mu_{\mathrm{Ge}} = \epsilon_\gamma$ as expected and $\mu_{\mathrm{Mn}} = (\epsilon_\gamma + \Delta_\mu) \in]-\infty, \Delta_\mu^{\max}[$, i.e., Mn atoms have a lower energy in the atom reservoir associated to the semigrand canonical potential than they would have by creating a new phase in the system. The value $\Delta_\mu^{\max}$ corresponds to the first stable compound containing Mn atoms. An equivalent remark can be done for the pure Mn phase.

When two phases γ and δ, with different compositions, are coexisting, the phase rule implies that Δ_μ is no longer independent. This correspond to the line segment extremities in the graph ϕ vs Δ_μ and

$$\mu_{\mathrm{Ge}} = \left(c^\delta_{\mathrm{Mn}}\epsilon_\gamma - c^\gamma_{\mathrm{Mn}}\epsilon_\delta\right)/\left(c^\delta_{\mathrm{Mn}} - c^\gamma_{\mathrm{Mn}}\right), \tag{10}$$

$$\mu_{\mathrm{Mn}} = \left(c^\delta_{\mathrm{Ge}}\epsilon_\gamma - c^\gamma_{\mathrm{Ge}}\epsilon_\delta\right)/\left(c^\delta_{\mathrm{Ge}} - c^\gamma_{\mathrm{Ge}}\right). \tag{11}$$

(b) *Application to the Ge-Mn phase diagram.* This comparison methodology was already used in a previous work to predict the metastability of a new Ge-Mn phase[50] in the Ge-rich part of the equilibrium phase diagram. In the present work we extend our analysis to the entire phase diagram, including also HT and HP phases. We also investigate the sensitivity to the freezing (Fig. 6) or not (Fig. 7) of semicore electrons. The reduced semigrand canonical potential ϕ is reported on each figure for STP, HT, and HP phases [panels (a), (b), and (c), respectively). For readability reasons, and since we only want to address relative stability issues, we have applied a shift to both the x and y axes of the diagrams, so that the origin of the (ϕ,Δ_μ) plan is at the intersection of the lines for diamond Ge and Mn_α.[66] Such a simple shift can be achieved by rewriting Eq. (5) as

$$\phi(\Delta_\mu) = \epsilon - \left(\frac{\epsilon_{\mathrm{Ge}} + \epsilon_{\mathrm{Mn}}}{2}\right) + \left(\Delta_\mu - \epsilon_{\mathrm{Ge}} + \epsilon_{\mathrm{Mn}}\right)x, \tag{12}$$

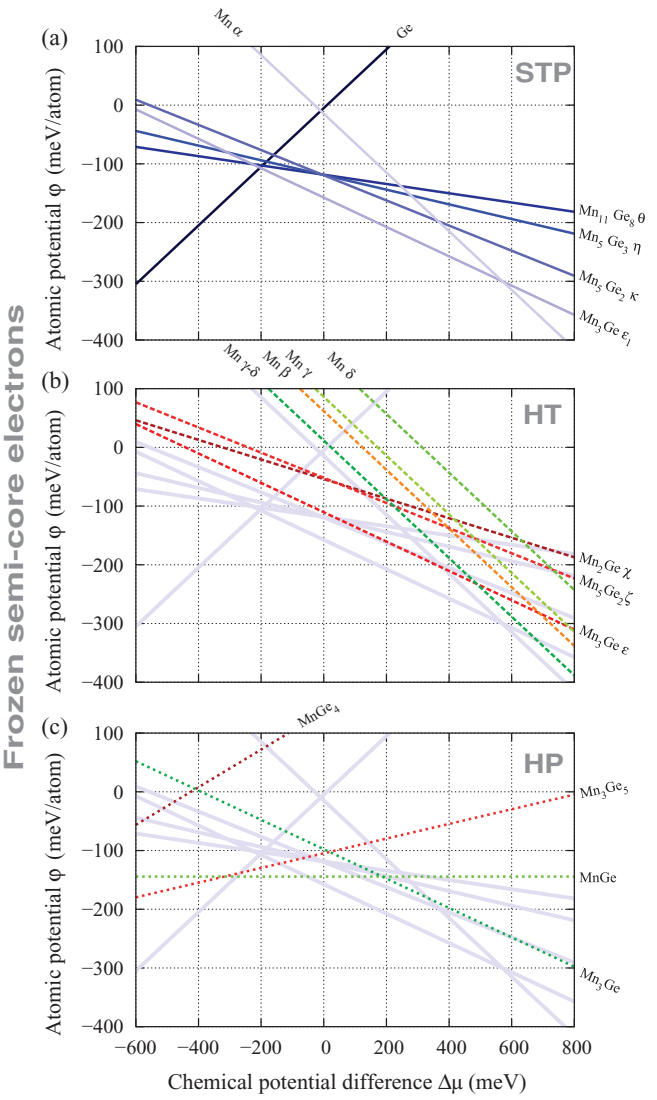

FIG. 6. (Color online) Evolution of the reduced semigrand canonical potential ϕ as a function of the difference of chemical potential Δ_μ [see Eq. (12)]. Simulations were performed without the semicore electrons. There is one straight line per Ge-Mn phase. The stable compound for each Δ_μ is the one with the lowest free energy. (a) STP phases; (b) HT phases (STP phases in light blue), and (c) HP phases (STP phases in light blue).

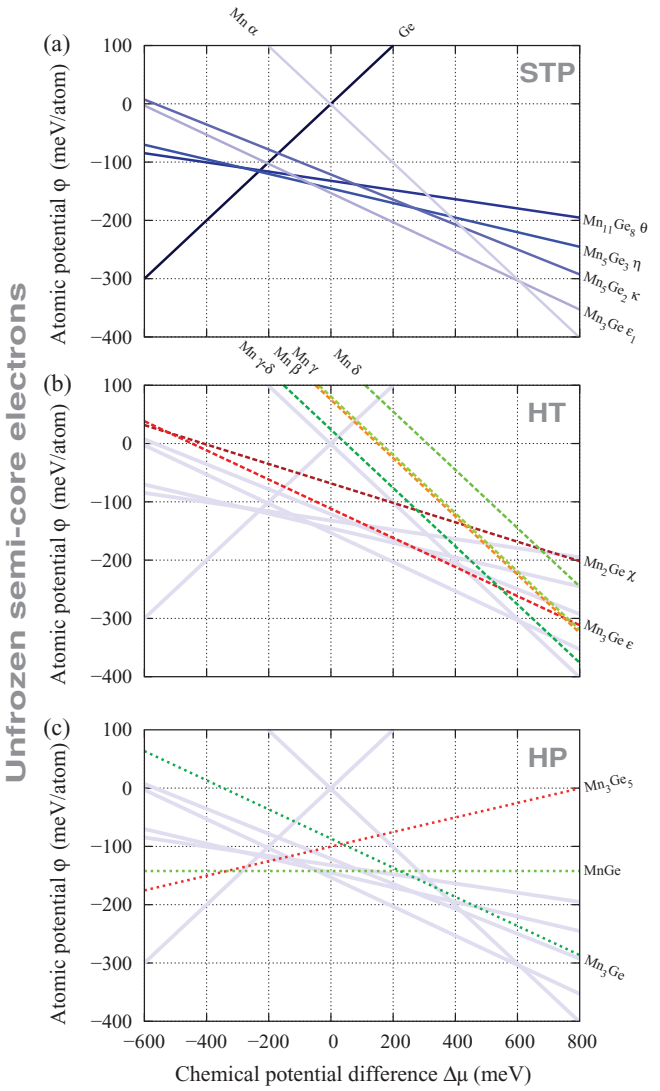

FIG. 7. (Color online) Evolution of the reduced semigrand canonical potential ϕ as a function of the difference of chemical potential Δ_μ [see Eq. (12)]. Simulations were performed with the semicore electrons as valence electrons. There is one straight line per Ge-Mn phase. The stable compound for each Δ_μ is the one with the lowest free energy. (a) STP phases; (b) HT phases (STP phases in light blue), and (c) HP phases (STP phases in light blue).

where ϕ and Δ_μ are now the shifted quantities, and where ϵ_{Ge} and ϵ_{Mn} are the *ab initio* energy per atom in the diamond Ge and Mn_α phases, respectively.

In order to reproduce the experimental phase diagram, there should be a stability domain for all of the six known phases stable in the STP conditions. A stability domain of a phase is simply a range in Δ_μ where the phase's line is the one with the lowest energy. If we look at Fig. 6(a), it would be the case only if the Mn_3Ge ϵ_1 compound had an energy $\sim$40 meV higher. Indeed, its low calculated energy prevents three phases [$Mn_{11}Ge_8$ θ, Mn_5Ge_3 (η), and Mn_5Ge_2 (κ)] from appearing stable in this diagram.

If we now look at the HT phases in Fig. 6(b), results are this time in perfect agreement with experiments since no metastable compound has a stability domain, even if Mn_3Ge

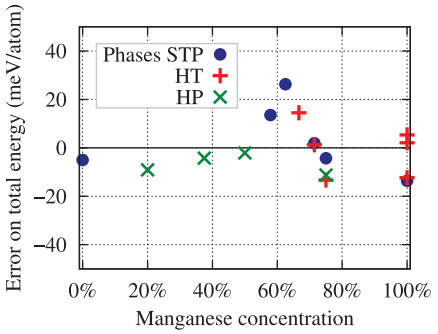

FIG. 8. (Color online) Error on energy induced by the freezing of semicore electrons, as a function of Mn concentration. Disks are STP phases, whereas crosses are HT or HP phases, red and green, respectively.

ϵ_1 were "corrected" by adding 40 meV. Concerning the HP phases in Fig. 6(c), the compounds MnGe B20 and Mn_3Ge_5 seem too low in energy by 30 and 20 meV/atom, respectively.

Finally, we would like to focus on the $MnGe_4$ compound, which has a noticeably higher energy than the other compounds: 180 meV/atom in the decomposition into $Mn_{11}Ge_8$ and diamond Ge (210 meV/atom for the unfaulted $MnGe_4$). In line with our previous remarks, we think this underlines a possible bad atomic structure description.

Among the 16 known Ge-Mn compounds that we have computed, three seem to be more difficult to simulate. If we now look at the Fig. 7, we can see that the relaxation of semicore electrons does not solve the problem, yet slightly diminishes its amplitude. Indeed, the three problematic compounds Mn_3Ge ϵ_1, MnGe B20, and Mn_3Ge_5 remain too low in energy, but this time by 40, 25, and 15 meV, respectively, while it was 40, 30, and 20 meV previously. We see three reasons that might explain the underestimation in energy: (i) the collinear approximation of magnetism and the lack of spin-orbit coupling; (ii) the approximation on exchange-correlation energy; and (iii) the fact that entropy is not taken into account [$T = 0$ in Eq. (5)].

The approximation on magnetism cannot account for the results since it can only lower the total energy of compounds such as MnGe B20 (noncollinear antiferromagnetic) as opposed to Mn_3Ge_5 (collinear ferromagnetic). That could only further worsen the results.

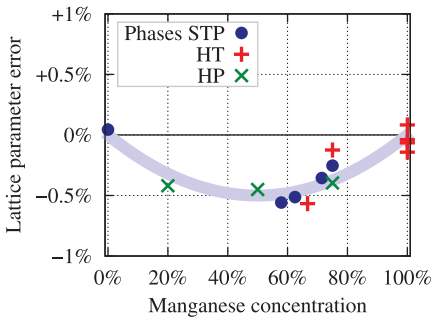

FIG. 9. (Color online) Error on the lattice parameter induced by the freezing of semicore electrons, as a function of Mn concentration. Disks are STP phases, whereas crosses are HT or HP phases, red and green, respectively.

TABLE IV. Error on the lattice parameter induced by the freezing of semicore electrons for the Mn_5Ge_3 compound. s-c means that semicore electrons are not frozen, but explicitly taken into account in the calculation, in addition to the valence electrons.

Ge	Mn	a	c	Err_a	Err_c
		7.148	4.985	−0.5%	−1.3%
	s-c	7.163	4.987	−0.3%	−1.3%
s-c		7.155	4.989	−0.4%	−1.3%
s-c	s-c	7.186	5.009	0.0%	−0.9%
Exp		7.184	5.053		

On the other hand, the exchange-correlation functional can be the cause of this stability permutation. One would have to test other functionals to check the validity of this hypothesis, for example, hybrid functionals or the $+U$ formalism.[67] The first solution has been applied to the study of the Mn dimer,[68] and it seems that the addition of a Hartree-Fock part in the exchange term improves the results. However, correlations are known to be weaker in small molecules than in condensed matter. Thus, what works for the Mn dimer may fail for our compounds. Concerning the $+U$ formalism, it has a major drawback of being strongly dependent on the value of U which, being different for each phase, prevents any energy comparison between phases.

The third possible explanation is the effect of entropy. It was indeed shown for the Al_2Cu compound that entropy reverses the stability between C1 and C16 allotropic forms, compensating 15 meV/atom at temperatures higher than 200 °C.[69] In our case, GeMn alloys form at even higher temperatures, ∼700 °C. Thus, an inversion in stability of 40 meV/atom seems possible. Unfortunately, the evaluation of the vibrational and configurational terms of entropy are both close to impossible in this system. The first term would require the phonon density of state of all alloys, beyond reach of computation for cells as big as 76 atoms. The second term would require the calculation of the energy of the different defects for each alloy.

D. Impact of semicore electrons

In order to assess more precisely the effect of freezing the semicore electrons in the calculations, the induced errors on energy and lattice parameter are plotted in Figs. 8 and 9, respectively.

The error on energy resulting from the freezing of semicore electrons is lower than 20 meV/atom, except for Mn_5Ge_3, for which it reaches 26 meV/atom (see Fig. 8). We can notice that the error is bigger in compounds whose Mn concentration is ∼60%. This tendency is the same regarding the error on lattice parameter (see Fig. 9), with a maximal difference of −0.5%. This difference in behavior can be attributed to the polarizability of semicore electrons, which reacts differently for compounds such as Mn_5Ge_3 and $Mn_{11}Ge_8$, whose mean moments are higher than $2.5\mu_B$.

The error caused by freezing the semicore electrons (20 meV/atom, <0.5%) is smaller than the error due to exchange-correlation energy and entropy (40 meV/atom, 2.5%). Yet it is not negligible, and calculations requiring precision should be performed with the inclusion of semicore electrons. We have also tested an intermediate solution on the Mn_5Ge_3 compound, in which semicore electrons are taken into account only for one of the two species (Mn or Ge). It appears that the results are only half improved, as shown on Table IV, and that semicore electrons of both Mn and Ge are needed, none playing a clearly dominant role.

V. CONCLUSION

A review of the known compounds of the Ge-Mn phase diagram was presented, based on an extensive study of these 16 compounds. First, we discussed the almost linear relationship between alloy compacity and Mn concentration. Due to the different chemical behaviors of Mn and Ge atoms, the atomic density increases strongly with Mn concentration, pure Mn being almost twice as compact as diamond Ge. We have then tested the DFT calculations on this system, and we can draw the following conclusions: (i) The error on the lattice parameter caused by the DFT-GGA approximation is almost linearly correlated to the Mn concentration, ranging from +2% in pure Ge to −2.4% in pure Mn. Using the LDA approximation causes much larger errors (for instance ,−5.1% as compared to −2.4% for Mn α lattice parameter), especially in the presence of Mn. (ii) Here magnetism is well reproduced, even when the calculated lattice parameters are used instead of the experimental values. (iii) A simple thermodynamical approach has been presented and allows a comparison between our DFT calculations and the experimental phase diagram. Good agreement has been obtained for all compounds except for three alloys. In these latter cases, the error reaches only 40 meV/atom. This error results from both the approximations made on exchange-correlation energy, and on a missing entropy term that was not taken into account in this study. (iv) The freezing of semicore electrons in the pseudopotential causes an error of lower than 0.5% on the lattice parameter, $0.1\mu_B$/Mn on the magnetic moments, and up to 26 meV/atom on the energy. Obtaining a significant increase in precision requires that one takes into account all semicore electrons (both for Mn and Ge), thus leading to a computation time that is almost ten times larger.

We can conclude that the DFT method is suitable to study the Ge-Mn systems, provided that resulting computational errors are taken into account. Calculations with frozen semicore electrons are computationally faster and yield physically acceptable results, yet require efficient pseudopotentials. In addition, PAW formalism is recommended, whereas the HGH pseudopotential for Mn without a semicore electron is physically inappropriate.

Lastly, our calculations show that $MnGe_4$ compound as described in Ref. 45 has a behavior inconsistent with experimental results, pointing toward a possible error in the description of its atomic structure.

ACKNOWLEDGMENT

The calculations were performed at the CEA supercomputing center (CCRT).

*pascal.pochet@cea.fr

[1] Y. D. Park, A. T. Hanbicki, S. C. Erwin, C. S. Hellberg, J. M. Sullivan, J. E. Mattson, T. F. Ambrose, A. Wilson, G. Spanos, and B. T. Jonker, Science **295**, 651 (2002).

[2] S. Ahlers, D. Bougeard, N. Sircar, G. Abstreiter, A. Trampert, M. Opel, and R. Gross, Phys. Rev. B **74**, 214411 (2006).

[3] C. Bihler, C. Jaeger, T. Vallaitis, M. Gjukic, M. S. Brandt, E. Pippel, J. Woltersdorf, and U. Gösele, Appl. Phys. Lett. **88**, 112506 (2006).

[4] D. Bougeard, S. Ahlers, A. Trampert, N. Sircar, and G. Abstreiter, Phys. Rev. Lett. **97**, 237202 (2006).

[5] T. Devillers, M. Jamet, A. Barski, V. Poydenot, P. Bayle-Guillemaud, E. Bellet-Amalric, S. Cherifi, and J. Cibert, Phys. Rev. B **76**, 205306 (2007).

[6] M. Jamet, A. Barski, T. Devillers, V. Poydenot, R. Dujardin, P. Bayle-Guillemaud, J. Rothman, E. Bellet-Amalric, A. Marty, J. Cibert, R. Mattana, and S. Tatarenko, Nat. Mater. **5**, 653 (2006).

[7] P. D. Padova, J.-P. Ayoub, I. Berbezier, P. Perfetti, C. Quaresima, A. M. Testa, D. Fiorani, B. Olivieri, J.-M. Mariot, A. Taleb-Ibrahimi, M. C. Richter, O. Heckmann, and K. Hricovini, Phys. Rev. B **77**, 045203 (2008).

[8] A. Continenza, G. Profeta, and S. Picozzi, Appl. Phys. Lett. **89**, 202510 (2006).

[9] A. Continenza, G. Profeta, and S. Picozzi, Phys. Rev. B **73**, 035212 (2006).

[10] J. Hafner and D. Hobbs, Phys. Rev. B **68**, 014408 (2003).

[11] D. Hobbs, J. Hafner, and D. Spišák, Phys. Rev. B **68**, 014407 (2003).

[12] X. Luo, S. B. Zhang, and S.-H. Wei, Phys. Rev. B **70**, 033308 (2004).

[13] S. Picozzi, A. Continenza, and A. J. Freeman, Phys. Rev. B **70**, 235205 (2004).

[14] T. C. Schulthess and W. H. Butler, J. Appl. Phys. **89**, 7021 (2001).

[15] A. Stroppa, S. Picozzi, A. Continenza, and A. J. Freeman, Phys. Rev. B **68**, 155203 (2003).

[16] X. Gonze, G.-M. Rignanese, M. Verstraete, J.-M. Beuken, Y. Pouillon, R. Caracas, F. Jollet, M. Torrent, G. Zerah, M. Mikami, P. Ghosez, M. Veithen, J.-Y. Raty, V. Olevano, F. Bruneval, L. Reining, R. Godby, G. Onida, D. Hamann, D. Allan, G. Zerah, F. Jollet, M. Torrent, A. Roy, M. Mikami, P. Ghosez, J.-Y. Raty, and D. Allan, Z. Kristallogr. **220**, 558 (2005).

[17] M. Torrent, F. Jollet, F. Bottin, G. Zerah, and X. Gonze, Comput. Mater. Sci. **42**, 337 (2008).

[18] J. P. Perdew, K. Burke, and M. Ernzerhof, Phys. Rev. Lett. **77**, 3865 (1996).

[19] N. Holzwarth, A. Tackett, and G. Matthews, Comput. Phys. Commun. **135**, 329 (2001).

[20] C. Hartwigsen, S. Goedecker, and J. Hutter, Phys. Rev. B **58**, 3641 (1998).

[21] M. Krack, Theor. Chim. Acta **114**, 145 (2005).

[22] For consistency reasons, the smearing was also applied to diamond Ge despite the metallic character exhibited by DFT simulations (yet with a zero density of state at the Fermi level). That causes an error of 0.01% in the lattice parameter, 1% in the bulk modulus, and 0.02 meV/atom in the energy.

[23] Mn_α and Mn_5Ge_2 (ζ phase) have only been tested in one magnetic configuration because of the combinatorial complexity due to the number of nonequivalent atoms.

[24] T. B. Massalski, *Binary Alloy Phase Diagrams* (American Society for Metals, Materials Park, OH, 1990), Vol. 2.

[25] P. Villars, L. Calvert, and W. Pearson, *Pearson's Handbook of Crystallographic Data for Intermetallic Phases* (American Society for Metals, Materials Park, OH, 1985).

[26] A. Gokhale and R. Abbaschian, Bull. Alloy Phase Diagrams **11**, 460 (1990).

[27] P. Eckerlin and H. Kandler, in *Structure Data of Elements and Intermetallic Phases*, edited by K. H. Hellwege and Landolt Börnstein, New Series, Group III, Vol. 6 (Springer, Berlin, 1971), p. 15.

[28] P. Israiloff, H. Völlenkle, and A. Wittmann, Monatsh. Chem. **105**, 1387 (1974).

[29] N. Yamada, K. Maeda, Y. Usami, and T. Ohoyama, J. Phys. Soc. Jpn. **55**, 3721 (1986).

[30] L. Castelliz, Monatsh. Chem. **84**, 765 (1953).

[31] J. B. Forsyth and P. J. Brown, J. Phys. Condens. Matter **2**, 2713 (1990).

[32] T. Ohba, K. Ueyama, Y. Kitano, and Y. Komura, Acta Crystallogr. Sect. C **40**, 576 (1984).

[33] N. Yamada, J. Phys. Soc. Jpn. **59**, 273 (1990).

[34] N. Yamada, S. Funahashi, F. Izumi, M. Ikegame, and T. Ohoyama, J. Phys. Soc. Jpn. **56**, 4107 (1987).

[35] G. Kadar and E. Kren, Int. J. Magn. **1**, 143 (1971).

[36] T. Ohoyama, J. Phys. Soc. Jpn. **16**, 1995 (1961).

[37] A. C. Lawson, A. C. Larson, M. C. Aronson, S. Johnson, Z. Fisk, P. C. Canfield, J. D. Thompson, and R. B. V. Dreele, J. Appl. Phys. **76**, 7049 (1994).

[38] M. Ellner, J. Appl. Crystallogr. **13**, 99 (1980).

[39] Y. Komura, T. Ohba, K. Kifune, H. Hirayama, T. Tagai, N. Yamada, and T. Ohoyama, Acta Crystallogr. Sect. C **43**, 7 (1987).

[40] T. Ohba, K. Kifune, and Y. Komura, Acta Crystallogr. Sect. B **43**, 489 (1987).

[41] Y. Komura and H. Hirayama, Acta Crystallogr. Sect. A **37**, C184 (1981).

[42] C. B. Shoemaker, D. P. Shoemaker, T. E. Hopkins, and S. Yindepit, Acta Crystallogr. Sect. B **34**, 3573 (1978).

[43] J. B. Goodenough, Phys. Rev. **120**, 67 (1960).

[44] M. Hortamani, Ph.D. thesis, Faculty of Physics at the Freie Universität, Berlin, 2006.

[45] H. Takizawa, T. Sato, T. Endo, and M. Shimada, J. Solid State Chem. **88**, 384 (1990).

[46] H. Takizawa, T. Sato, T. Endo, and M. Shimada, J. Solid State Chem. **68**, 234 (1987).

[47] H. Takizawa, T. Sato, T. Endo, and M. Shimada, J. Solid State Chem. **73**, 40 (1988).

[48] H. Takizawa, T. Yamashita, K. Uheda, and T. Endo, J. Phys. Condens. Matter **14**, 11147 (2002).

[49] The compacity is the ratio between the number of atoms and the volume of the unit cell, called "atomic density" in physics, or "number density."

[50] E. Arras, I. Slipukhina, M. Torrent, D. Caliste, T. Deutsch, and P. Pochet, Appl. Phys. Lett. **96**, 231904 (2010).

[51] W. Zhu, H. H. Weitering, E. G. Wang, E. Kaxiras, and Z. Zhang, Phys. Rev. Lett. **93**, 126102 (2004).

[52] A. Stroppa, G. Kresse, and A. Continenza, Appl. Phys. Lett. **93**, 092502 (2008).

[53] P. Eckerlin and H. Kandler, in *Structure Data of Elements and Intermetallic Phases*, edited by K. H. Hellwege, Landolt Börnstein, New Series, Group III, Vol. 6 (Springer, Berlin, 1971), p. 6.

[54]T. Ohba, N. Watanabe, and Y. Komura, Acta Crystallogr. Sect. B **40**, 351 (1984).

[55]P. Eckerlin and H. Kandler, in *Structure Data of Elements and Intermetallic Phases*, edited by K. H. Hellwege and Landolt Börnstein, New Series, Group III, Vol. 6 (Springer, Berlin, 1971), pp. 626–627.

[56]μ_C/μ_S is known to be larger than 1 for itinerant magnetism.

[57]P. Rhodes and E. Wohlfarth, Proc. R. Soc. London A **273**, 247 (1963).

[58]I. Slipukhina, E. Arras, P. Mavropoulos, and P. Pochet, Appl. Phys. Lett. **94**, 192505 (2009).

[59]It has been shown for Mn_5Ge_3C (see Ref. 60) that exchange interactions within Mn_{II} are ferromagnetic, with or without the presence of an interstitial.

[60]A. Burkhanov, V. Novogrudskiy, and I. Fakidov, Fiz. Met. Metalloved. **42**, 889 (1976).

[61]H. Nakamura, K. Yoshimoto, M. Shiga, M. Nishi, and K. Kakurai, J. Phys. Condens. Matter **9**, 4701 (1997).

[62]M. Laradji, D. P. Landau, and B. Dünweg, Phys. Rev. B **51**, 4894 (1995).

[63]R. A. Alberty, Pure Appl. Chem. **73**, 1349 (2001).

[64]H. B. Callen, *Thermodynamics and an Introduction to Thermostatistics* (Wiley, New York, 1985).

[65]R. Balian, *From Microphysics to Macrophysics* (Springer, Berlin, 1991), Vol. 1, Chap. 6.3.

[66]To facilitate comparison between the $\phi(\Delta_\mu)$ graphs, the origin has been first set for the calculation that includes the semicore electrons. The origin for the calculation with frozen semicore electrons was then chosen to minimize the overall differences between the boundaries of the phase transitions.

[67]A. Stroppa, G. Kresse, and A. Continenza, Phys. Rev. B **83**, 085201 (2011).

[68]S. Yamanaka, T. Ukai, K. Nakata, R. Takeda, M. Shoji, T. Kawakami, T. Takada, and K. Yamaguchi, Int. J. Quantum Chem. **107**, 3178 (2007).

[69]C. Wolverton and V. Ozoliņs, Phys. Rev. Lett. **86**, 5518 (2001).